



Evaluation of Cytotoxic Effect in Ag/ZnO Nanocomposites on Human Myelogenous Leukaemia

S. Magara Jothi Lakshmi ^{a++} and S. G. Rejith ^{a++*}

^a St. Xavier's College (Autonomous), affiliated to Manonmaniam Sundaranar University, Tirunelveli 627002, Tamil Nadu, India.

Authors' contributions

This work was carried out in collaboration between both authors. Author SMJL conceptualized the study, performed methodology, did formal analysis, investigation, data visualization and wrote original draft. Author SGR conceptualized the study, wrote, reviewed and edited the manuscript, supervised the study. Both authors read and approved the final manuscript.

Article Information

DOI: <https://doi.org/10.56557/upjoz/2024/v45i124109>

Open Peer Review History:

This journal follows the Advanced Open Peer Review policy. Identity of the Reviewers, Editor(s) and additional Reviewers, peer review comments, different versions of the manuscript, comments of the editors, etc are available here: <https://prh.mbimph.com/review-history/3533>

Original Research Article

Received: 11/03/2024

Accepted: 15/05/2024

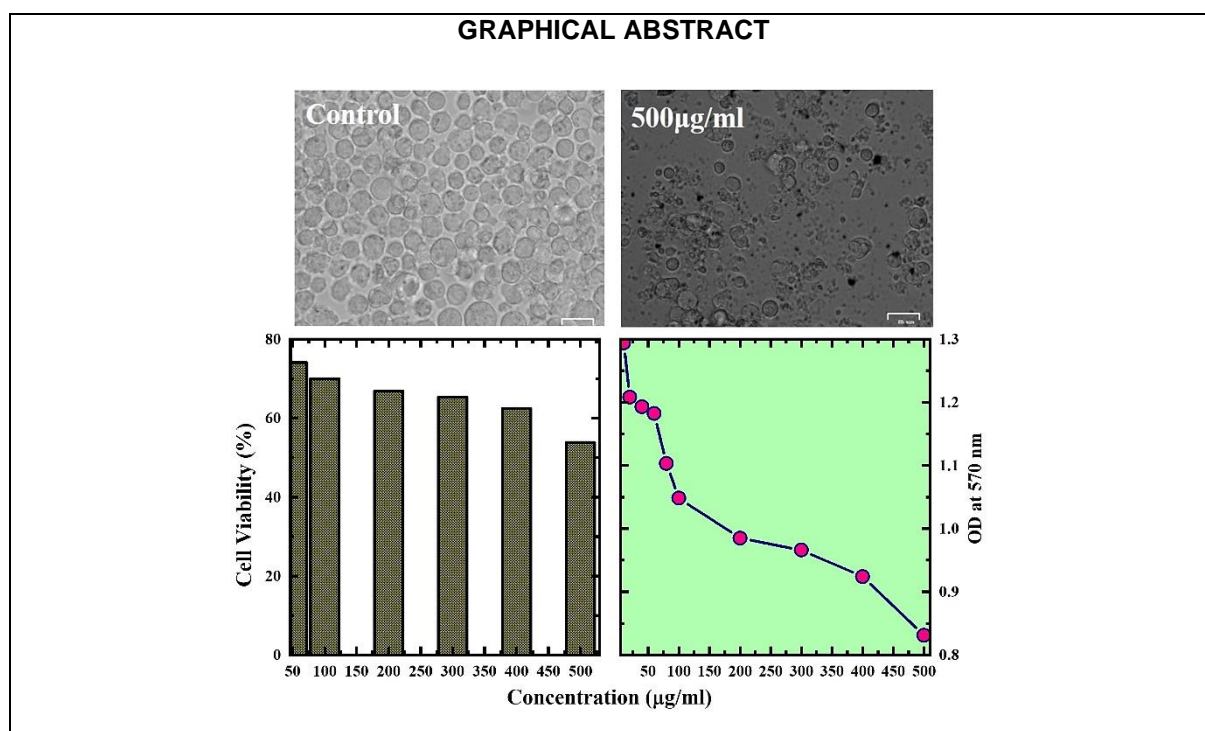
Published: 21/05/2024

ABSTRACT

The Ag/ZnO nanocomposite was successfully synthesized through the co-precipitation method, as confirmed by the simultaneous presence of Ag and ZnO reflections in powder X-ray diffraction analysis, validating its formation. Analysis using FESEM revealed an average particle size of around 22 nm and displayed a unique flower-like morphology, indicating a distinctive self-assembly and growth pattern of the nanocomposite. Structural composition and functional groups were studied using FT-IR spectroscopy. The nanocomposite exhibited direct and indirect band gaps of 3.06 and 3.00 eV, respectively, determined through UV-Vis NIR spectrometry and Tauc plot analysis. Evaluation of the cytotoxic effect on K562 (human myelogenous leukaemia) cells demonstrated a concentration-dependent decrease in cell viability, highlighting the potential of the nanocomposite to induce cytotoxic effects on these cancer cells.

⁺⁺ Research Scholar Reg. No. 20121282132009;

*Corresponding author: Email: rejithsg23@gmail.com;



Keywords: Ag/ZnO; nanocomposite; co-precipitation; band gap; cytotoxicity.

1. INTRODUCTION

The emergence of metal-metal oxide nanocomposites has sparked significant interest in the fields of materials science and nanotechnology. These hybrid structures, amalgamating the distinct properties of metals and metal oxides, present a versatile platform characterized by augmented functionalities and customized attributes suitable for a diverse range of applications especially in biomedical applications [1]. Zinc and copper are implicated in the mechanism responsible for eliminating pathogens within eukaryotic cells, utilizing oxidative stress to eradicate engulfed microbes. Remarkably, even at low concentrations, metals like gold, silver, and mercury exhibit pronounced toxicity to bacteria, showcasing broad-spectrum antibacterial effects [2].

Zinc oxide (ZnO), renowned for its diverse nanostructures, exhibits distinctive semiconducting, optical, and piezoelectric properties [3,4]. Consequently, nanomaterials derived from ZnO have been extensively explored for a wide range of applications, including nano-electronics, nano-optical devices, energy storage, cosmetic products, and nano-sensors [5-11]. ZnO is identified as a wide band gap semiconductor (3.37 eV) with a high exciton binding energy (60meV), resulting in efficient

blue and near-UV excitonic emission [12]. The stability and inherent ability of ZnO to absorb UV irradiation have led to its approval by the Food and Drug Administration (FDA) for use in sunscreens. A key attribute of ZnO nanomaterials is their low toxicity and biodegradability. Zn²⁺ plays a crucial role as a trace element in various metabolic processes for adults. Chemically, the surface of ZnO is rich in -OH groups, offering convenient opportunities for functionalization with diverse surface decorating molecules. Under specific conditions, such as acidic environments like tumor cells and the tumor microenvironment, ZnO can gradually dissolve. This dissolution can also take place in strong basic conditions when the surface is in direct contact with the solution. Due to these favourable properties, ZnO nanomaterials have garnered significant attention in biomedical applications.

Metal and metal oxide nanoparticles have attracted considerable attention as potent antibacterial agents, owing to their heightened reactivity arising from an exceptionally high surface area-to-volume ratio [13]. As a result, the potential of Ag/ZnO nanocomposites can be leveraged for applications in environmental health, particularly in the creation of antimicrobial compounds for water disinfection. To harness synergies, diverse alloys have been synthesized,

showcasing superior antimicrobial effects against bacterial drug resistance during water disinfection [14,15]. The remarkable efficiency of Ag/ZnO nanocomposites is attributed to their plasmonic properties and interfacial electron exchange processes. Moreover, in comparison to pure ZnO nanoparticles, the effectiveness of Ag/ZnO nanocomposites has been evaluated for their heightened release of silver and zinc ions in aqueous solutions, increased stability, enhanced reusability, and prolonged bactericidal effects [16-20].

The objective of this study is to conduct a detailed exploration into the synthesis and characterization of an Ag/ZnO nanocomposite using a co-precipitation method, aiming to uncover the intricate interactions between silver and zinc oxide at the nanoscale. Through a comparative analysis with previous studies, we seek to validate and expand upon our findings, shedding light on the evolving landscape of nanocomposite research. Utilizing a range of characterization techniques including XRD, FESEM, EDS, FTIR, UV-Vis spectroscopy, and MTT assay, our goal is to provide a comprehensive understanding of the structural, morphological, compositional, and functional aspects of the Ag/ZnO nanocomposite. By placing our research within the broader context of nanomaterial advancements and biomedical applications, we aim to contribute valuable insights that could lead to innovative solutions across diverse fields, from nano-electronics to healthcare, thereby pushing the boundaries of scientific exploration and leveraging nanotechnology for societal benefit.

2. MATERIALS AND METHODS

2.1 Synthesis of Ag/ZnO Nanocomposite by Co-Precipitation Method

Ag/ZnO nanocomposite was synthesized through co-precipitation method. Zinc di-nitrate hexahydrate ($\text{ZnO}(\text{NO}_3)_2 \cdot 6\text{H}_2\text{O}$) (0.4mol) was dissolved in a mixture of 40mL ethanol and 10mL water and stirred for 2 hours. Subsequently, Silver nitrate (AgNO_3) (0.045mol) and NaOH (10 mL) were added dropwise, followed by the addition of NaBH_4 (0.5 mg) dissolved in 5mL ice-cold water. Throughout this process, the precipitate changed from colourless to brownish at pH = 12, indicating the formation of the nanocomposite. The resulting product was collected through centrifugation at 6000 rpm for 1 hour, subjected to several washes with distilled

water and ethanol, and then dried at 100°C for 24 hours to yield the Ag/ZnO nanocomposite. Powder diffraction data of Ag/ZnO nanocomposite was recorded with Bruker Eco D8 Advance X-ray diffractometer. Morphological analysis of Ag/ZnO nanocomposite was performed with ZEISS EVO 18 Model. The infrared (IR) spectra were obtained within the 4000-500 cm^{-1} range using a BRUKER-ALPHA-Platinum-ATR IR spectrophotometer. Additionally, the ultraviolet-visible (UV-Vis) spectrum was recorded using a Perkin-Elmer LAMBDA 950UV-VIS-NIR spectrophotometer.

2.2 Cell Culture

K562 human myelogenous leukaemia cells were obtained from National Centre for Cell Science (NCCS), Pune. The cells were maintained in RPMI liquid medium supplemented with 10% fetal bovine serum (FBS), 100 $\mu\text{g}/\text{ml}$ streptomycin, and 100 $\mu\text{g}/\text{ml}$ penicillin. Cultures were maintained at 37°C in a 5% CO_2 environment.

2.3 MTT Assay

The MTT assay was employed to assess the in vitro cytotoxicity of the test sample against K562 cells. Briefly, K562 cells were harvested and placed in a 15 ml tube. Subsequently, the cells were exposed to varying concentrations of the test sample in serum-free RPMI medium, seeded into a 96-well tissue culture plate at a density of 1×10^5 cells/ml (200 μL per well). The cells were then incubated for 24 hours at 37°C in a humidified 5% CO_2 incubator, with each sample replicated three times. After the incubation period, 10 μL of 5mg/ml MTT was added to each well, and the cells were further incubated for 2-4 hours until purple precipitates were clearly visible under an inverted microscope. Following this, the medium was aspirated, and 220 μL of MTT was removed from the wells, followed by a wash with 200 μL of 1X PBS. Additionally, 100 μL of DMSO was added, and the plate was vigorously shaken for five minutes to dissolve the formazan crystals. The percentage of cell viability and the IC50 value were calculated using Graph Pad Prism 6.0 software (USA) and the absorbance for each well was measured at 570 nm using a microplate reader (Thermo Fisher Scientific, USA).

2.4. Antibacterial Assay

The antimicrobial effectiveness of the synthesized Ag/ZnO nanocomposites was

assessed against both gram-positive (*Staphylococcus aureus* - 902) and gram-negative (*Escherichia coli* - 443) bacterial strains using the Agar well diffusion method. Nutrient agar medium in Petri plates was inoculated with a 24-hour culture of bacterial strains adjusted to a 0.5 OD value as per the McFarland standard. Wells were then created, and different concentrations of the sample (500, 250, 100, and 50 $\mu\text{g/ml}$) were added. After incubation at 37°C for 24 hours, the antibacterial activity was evaluated by measuring the diameter of the inhibition zone around the wells. Gentamicin antibiotic was used as a positive control, and the data were analyzed using Graph Pad Prism 6.0 software (USA).

3. RESULTS AND DISCUSSION

3.1 Powder X-ray Diffraction

Fig. 1 illustrates the powder X-ray diffraction patterns of pristine ZnO (Top) and Ag (Middle) nanoparticles synthesized using the co-precipitation method. The diffraction peaks corresponding to pure ZnO are observed at 2θ values of 31.65°, 34.32°, 36.14°, 47.48°, 56.49°, 62.78°, 66.36°, 67.85°, 68.99°, 72.41°, and 76.96°. These peaks align with the crystal planes of (100), (002), (101), (102), (110), (103), (200), (112), (201), (004), and (202) in the hexagonal wurtzite structure of ZnO nanoparticles, in accordance with JCPDS file no. 36-1451, as indicated by vertical bars in Fig. 1 [16]. Similarly, the diffraction peaks of pure Ag are observed at 2θ values of 38.13°, 44.30°, 64.49°, and 77.44°, corresponding to the crystal planes of (111), (200), (220), and (311), respectively, in the Face-Centered Cubic structure. This matches well with JCPDS file no. 04-0783, as indicated by vertical bars in Fig. 1 (Bottom) [17]. The average crystallite size, calculated using Scherer's Equation, is determined to be 16 nm for pure ZnO and 13 nm for Ag, as detailed in Table 1.

The X-ray diffraction (XRD) pattern of the Ag/ZnO nanocomposites synthesized through co-precipitation method as shown in Fig. 1 (Bottom), revealed distinctive peaks at specific 2θ values, indicating the crystallographic nature of the sample. The peaks at 31.4°, 34°, 35.9°, 47.2°, 56.2°, 66°, 67.6° and 68.8° correspond to the hexagonal wurtzite structure of Zinc Oxide (ZnO), as evidenced by a strong match with JCPDS Card No. 36-1451 [16]. These results affirm the crystalline nature of the ZnO phase in the nanocomposite. Concomitantly, peaks at

37.8°, 43.9°, 64.2° and 77.1° were observed, aligning well with the Face-Centered Cubic structure of Silver (Ag), validating the presence of metallic silver in the nanocomposite material (JCPDS Card No. 04-0783) [17]. The simultaneous presence of ZnO and Ag phases confirms the successful formation of Ag/ZnO nanocomposites. The distinct peaks associated with each phase indicate that the crystalline integrity of the individual components has been retained during the synthesis process. The peak intensities, measured in arbitrary units, provide insights into the relative abundance of the crystalline phases in the nanocomposites.

Fig. 2 shows the Williamson-Hall plot for the estimation of crystallite size of pure ZnO and Ag nanoparticles and the crystallite sizes are listed as 28 nm and 20 nm in Tables 2 and 3, respectively, appear somewhat larger than those calculated from Scherer's formula. This discrepancy can arise due to the different assumptions and mathematical models used in these two methods. Scherer's formula simplifies the crystallite size calculation based on diffraction peak broadening, assuming ideal conditions such as spherical crystallites, negligible strain effects, and homogeneous microstructure. On the other hand, the Williamson-Hall method considers additional factors like lattice strain and microstructural imperfections, leading to potentially larger estimated sizes.

3.2 FESEM & EDS Analysis

Field-Emission Scanning Electron Microscope (FESEM) serve as invaluable tools for nanomaterial characterization. FESEM allows for high-resolution imaging of nanoscale structures, providing detailed information about morphology, size, and distribution of nanoparticles or features within a sample. It enables researchers to observe surface topography, analyze particle agglomeration, and investigate structural changes under different conditions, crucial for understanding material properties and behaviour. FESEM image of the Ag/ZnO nanocomposite reveal a distinctive flower-like morphology, showcasing a visually striking and intricate structure as shown in Fig. 3. The average particle size, determined from the FESEM analysis, is measured to be approximately 22nm. The flower-like morphology observed in the images suggests a unique self-assembly and growth pattern of the Ag/ZnO nanocomposite. The formation of such structures can be

attributed to various factors, including the nature of the precursors, reaction conditions, and the presence of nucleation sites. The intricate petal-like features indicate a high degree of complexity in the nanostructure, which is crucial for tailoring the material's properties [18]. The EDS spectrum

confirms the presence of Zn, Ag, and O in the samples, facilitating elemental analysis as illustrated in Fig. 4. The chemical compositions, expressed in weight percentages (wt.%), reveal that Zn, Ag, and O constitute 23.17 wt.%, 61.72 wt.%, and 15.10 wt.%, respectively.

Table 1. Two theta (2θ), FWHM and crystallite size of pure ZnO and Ag nanoparticles estimated from Scherer's Equation

Sample	Two Theta (deg.)	FWHM (deg.)	Crystallite Size (nm)	Average size (nm)
ZnO	31.65	0.4222	18	16
	34.32	0.3388	22	
	36.14	0.4399	17	
	47.48	0.5492	13	
	56.49	0.5299	13	
	62.78	0.5222	13	
Ag	38.13	0.3979	19	13
	44.30	0.6026	12	
	64.49	0.5163	13	
	77.44	0.6437	10	

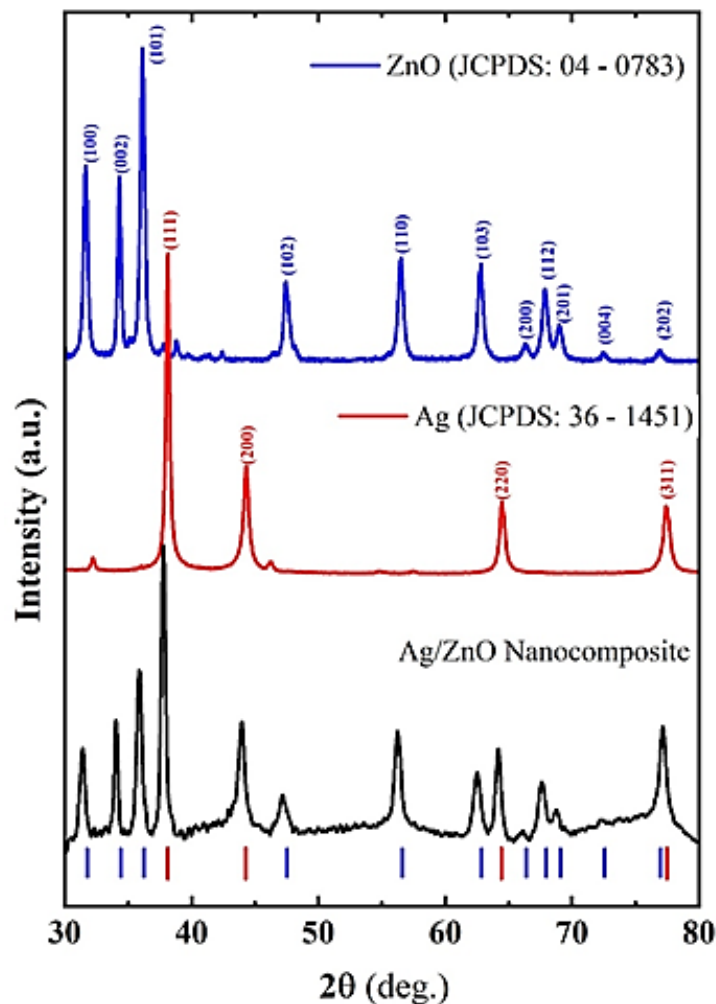


Fig. 1. Powder X-ray diffraction pattern of pure ZnO, Ag and Ag/ZnO nanoparticles

Table 2. Two theta (2θ), FWHM and crystallite size of pure ZnO nanoparticles estimated from Williamson-Hall (W-H) method

Sample	Two Theta (deg.)	Theta (Radian)	FWHM (deg.)	FWHM (Radian)	$4\sin\theta$	$\beta \cdot \cos\theta$	Crystallite Size (nm)
ZnO	31.65	0.276	0.4222	0.007363	1.090037	0.007084495	28
	34.32	0.299	0.3388	0.005909	1.178259	0.005646513	
	36.14	0.315	0.4399	0.007672	1.239266	0.007294373	
	47.48	0.414	0.5492	0.009578	1.609098	0.008768885	
	56.49	0.493	0.5299	0.009241	1.893083	0.008140956	
	62.78	0.548	0.5222	0.009107	2.083925	0.007773589	

Table 3. Two theta (2θ), FWHM and crystallite size of pure Ag nanoparticles estimated from Williamson-Hall (W-H) method

Sample	Two Theta (deg.)	Theta (Radian)	FWHM (deg.)	FWHM (Radian)	$4\sin\theta$	$\beta \cdot \cos\theta$	Crystallite Size (nm)
Ag	38.13	0.331731	0.3979	0.006923	1.302721	0.006545993	20
	44.30	0.38541	0.6026	0.010485	1.503756	0.009716089	
	64.49	0.561063	0.5163	0.008984	2.128346	0.007606341	
	77.44	0.673728	0.6437	0.0112	2.495615	0.00875311	

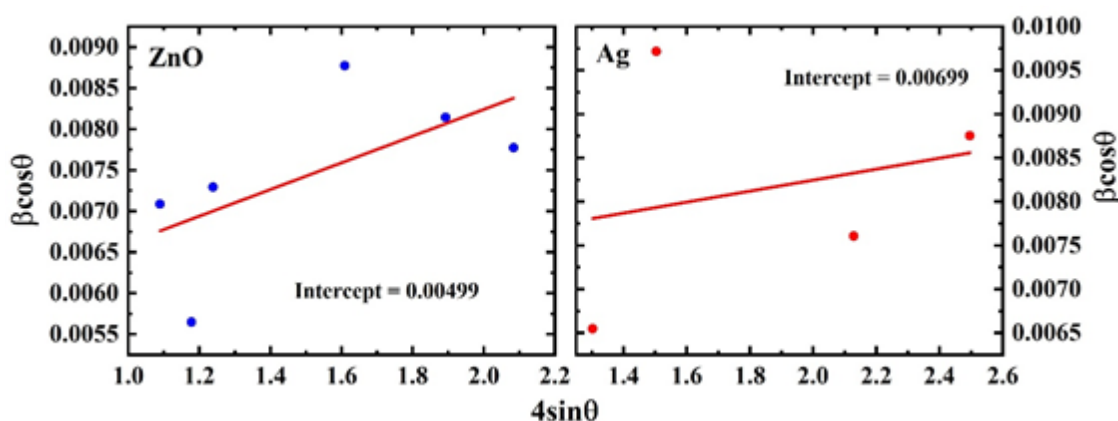


Fig. 2. Williamson-Hall plot for the estimation of crystallite size of pure ZnO and Ag nanoparticles

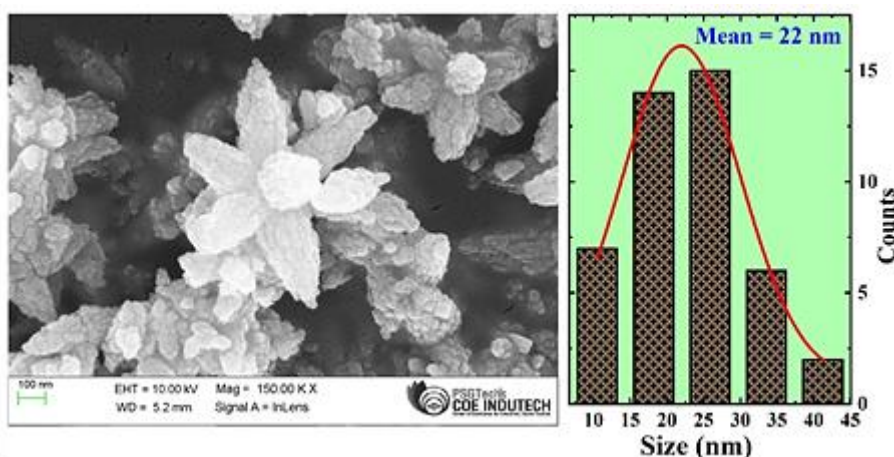


Fig. 3. FESEM morphological image of Ag/ZnO nanocomposite synthesized using co-precipitation method

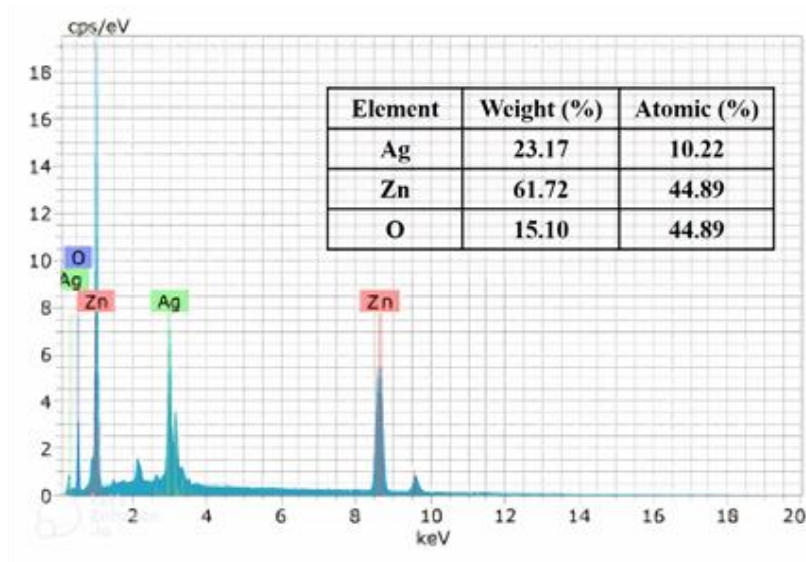


Fig. 4. EDS spectrum of Ag/ZnO nanocomposite synthesized using co-precipitation

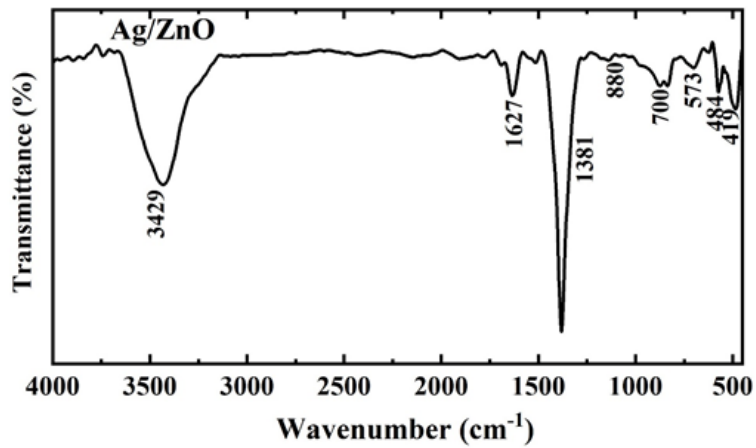


Fig. 5. FT-IR spectra of Ag/ZnO nanocomposite

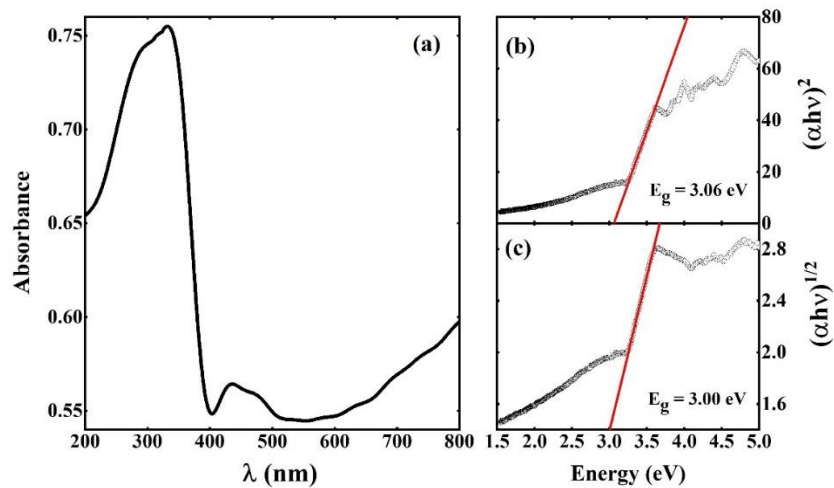


Fig. 6. UV-Vis absorbance spectra and Tauc plots of Ag/ZnO nanocomposite for (b) direct and (c) indirect band gap

3.3 FT-IR Spectroscopy Analysis

The functional groups present in the synthesized Ag/ZnO nanocomposite were investigated using FTIR spectroscopy over a range of 350-4500 cm^{-1} as shown in Fig. 5. The FTIR spectrum revealed distinct absorption features, including broad peaks at 3429 and 1627 cm^{-1} , corresponding to the stretching and bending modes, respectively, of the OH group from absorbed water. Additionally, a peak at 1381 cm^{-1} was identified as the bending vibration of C-H in the methyl group, while a minor peak at 880 cm^{-1} was attributed to the C-H out-of-plane bending from the alkene group. The absorption bands at 419, 484, and 573 cm^{-1} were assigned to the stretching modes of M-O (M = Ag & Zn) bonds [16].

3.4 UV-Vis-NIR Spectroscopy Analysis

The optical band gap of Ag/ZnO nanocomposite, synthesized through a co-precipitation method, was determined by analysing UV-Vis spectra within the 200-800nm range as shown in Fig. 6. The peak absorption wavelength, observed at 331nm, corresponds to the energy required for electron excitation in Ag/ZnO nanocomposites which is consistent with earlier reports [19]. Contrary to the visible range, the UV spectra of Ag/ZnO nanocomposites revealed peak absorption within the UV range, implying a higher

energy requirement for electron transitions between energy states. The determination of the optical band gap involved the utilization of the Tauc plot method, where absorbance was plotted against the corresponding wavelength (λ). This analysis yielded estimated values for both direct and indirect band gaps, measuring at 3.06 and 3eV, respectively. These values signify the minimum energy required for electrons to transition from the valence band to the conduction band in the material [20]. Similar band gap may be attributed to the modification of electronic structure, which is affected by hybridization of electronic states due to Ag-ZnO interactions.

3.5 Cytotoxicity Analysis

The inhibitory effects of chemically prepared Ag/ZnO nanocomposite on human cancer cells were evaluated using human myelogenous leukaemia K562 cells. The K562 cell line, commonly employed for assessing anti-cancer drug efficacy, was subjected to various concentrations (100, 200, 300, 400, and 500 $\mu\text{g}/\text{ml}$) of the nanocomposite as illustrated in optical image of Fig. 7. Optical microscopy offers insights into the overall appearance and optical properties of materials, including phase identification, grain boundaries, and defects. It is particularly useful for studying larger structures and assessing sample homogeneity.

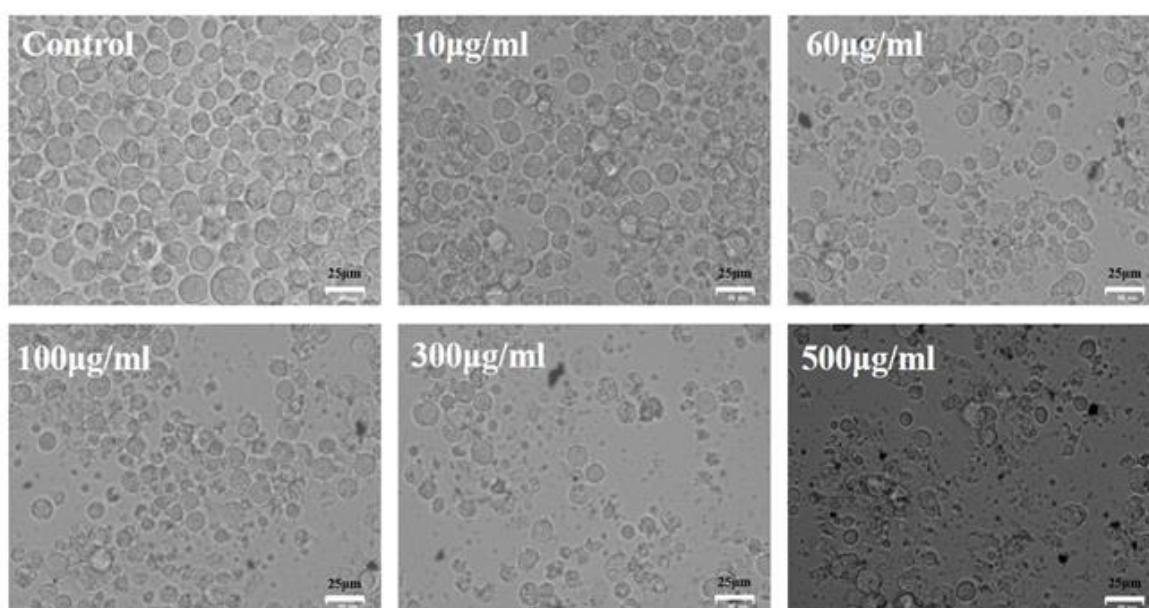


Fig. 7. Optical microscopy images and cell viability of K562 cells

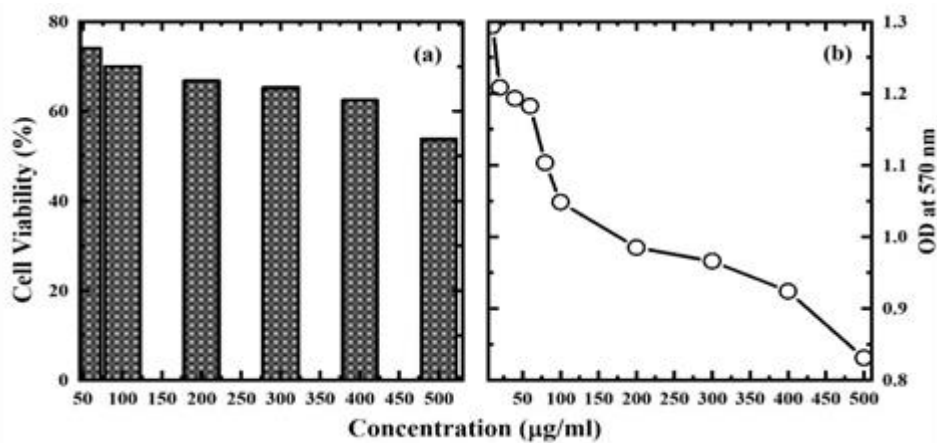


Fig. 8. (a) Cell viability of K562 cells treated with Ag/ZnO nanocomposites and (b) relative cell numbers were assessed through the absorbance (OD) values measured at 570 nm using MTT after 24 hours



Fig. 9. Antibacterial activities of Ag/ZnO nanocomposite synthesized using Co-Precipitation against *Staphylococcus aureus* and *E-Coli*

Fig. 8 (a) presents the anticancer outcomes represented as a percentage of cell viability. Cytotoxicity is a crucial aspect in practical biomedical applications. To evaluate the cytotoxic effects of Ag/ZnO nanocomposite on human myelogenous leukaemia K562 cancer cells, the 3-(4,5-dimethylthiazol-2-yl)-2,5-diphenyltetrazolium bromide (MTT) assay was employed. The percentage of cell viability was calculated using the following formula [21].

$$\text{Cell Viability} = \frac{\text{OD sample mean}}{\text{OD control mean}} \times 100$$

At lower concentrations (10µg/ml), the cell viability remained relatively unaffected, suggesting a tolerable response to the nanocomposite. The results revealed a

progressive decrease in cell viability from 86% to 53.8% as the concentration increased from 10 to 500µg/ml. The reduction in relative cell numbers, as indicated by the absorbance (OD) values measured at 570 nm using MTT after 24 hours (Fig. 8 (b)), can be attributed to the concentration dependent cytotoxic effects of the Ag/ZnO nanocomposites.

Higher concentrations of the nanocomposite likely lead to increased exposure of the K562 cells to its cytotoxic components, resulting in a more pronounced impact on cell viability. Furthermore, the observations suggest that with higher drug concentrations, interactions with active target groups within the human myelogenous leukaemia K562 cells reached saturation, indicating the point at which maximum

cytotoxicity occurred. These findings underscore the significant potential of the Ag/ZnO nanocomposite to exhibit cytotoxic effects on human myelogenous leukaemia K562 cancer cells [22,23].

3.6 Antibacterial Activities of Ag/ZnO Nano-composites

The antibacterial efficacy of Ag/ZnO nanocomposites was assessed against both gram-positive (*Staphylococcus aureus* - 902) and gram-negative (*Escherichia coli* - 443) bacteria in the sample, as depicted in Fig. 9. Unfortunately, the sample exhibited no antibacterial activity against E-Coli and less active in *Staphylococcus aureus* in both the positive and negative control conditions [24,25]. This lack of antibacterial activity in the sample could be attributed to factors such as the specific composition, morphology, or surface properties of the nanocomposite, highlighting the need for further investigation into optimizing its antibacterial properties [26,27].

4. CONCLUSION

In summary, the present work successfully employed the co-precipitation method to synthesize the Ag/ZnO nanocomposite, as verified by the simultaneous presence of Ag and ZnO reflections in powder X-ray diffraction. The nanocomposite displayed intriguing characteristics, with a distinctive flower-like morphology observed through FESEM analysis, indicating a unique self-assembly and growth pattern. Structural composition and functional groups of the Ag/ZnO nanocomposite were thoroughly investigated using FT-IR spectroscopy. The analysis provided valuable insights into the chemical composition and bonding within the synthesized nanocomposite. Additionally, the nanocomposite's optical properties were evaluated, revealing direct and indirect band gaps of 3.06 and 3.00eV, respectively. This information was derived from a Tauc plot analysis based on UV-Vis NIR spectrometry, shedding light on the material's electronic structure and potential applications in electronic devices. The practical implications of the present study were further emphasized through the concentration-dependent cytotoxicity assessment on K562 (human myelogenous leukaemia) cells. The results demonstrated a substantial decrease in cell viability with increasing concentrations of Ag/ZnO nanocomposites. This highlights the promising

potential of the nanocomposite as an effective agent in inducing cytotoxic effects on human myelogenous leukaemia K562 cancer cells. Overall, findings in this study contribute valuable insights into the synthesis, characterization, and potential applications of the Ag/ZnO nanocomposite in the biomedical field.

ACKNOWLEDGEMENTS

The Author, S. Magara Jothi Lakshmi acknowledges Nano Lab, Department of Physics, Sri Sarada College for Women (An Autonomous Institution), Tirunelveli - 627 011 for providing experimental facilities.

COMPETING INTERESTS

Authors have declared that no competing interests exist.

REFERENCES

1. Ray C, Pal T. Retracted article: Recent advances of metal-metal oxide nanocomposites and their tailored nanostructures in numerous catalytic applications. *Journal of Materials Chemistry A*. 2017;5(20):9465-87.
2. Pachaiappan R, Rajendran S, Show PL, Manavalan K, Naushad M. Metal/metal oxide nanocomposites for bactericidal effect: A review. *Chemosphere*. 2021;272:128607.
3. Moezzi A, McDonagh AM, Cortie MB. Zinc oxide particles: Synthesis, properties and applications. *Chemical Engineering Journal*. 2012;185:1-22.
4. Prasongsook P, Lachom V, Kenyota N, Laokul P. Characterization and photocatalytic performance of hollow zinc oxide microspheres prepared via a template-free hydrothermal method. *Materials Chemistry and Physics*. 2019;237:121836.
5. Sharma DK, Shukla S, Sharma KK, Kumar V. A review on ZnO: Fundamental properties and applications. *Materials Today: Proceedings*. 2022;49:3028-35.
6. Raha S, Ahmaruzzaman M. ZnO nanostructured materials and their potential applications: Progress, challenges and perspectives. *Nanoscale Advances*. 2022;4(8):1868-925.
7. Noman MT, Amor N, Petru M. Synthesis and applications of ZnO nanostructures (ZONSS): A review. *Critical Reviews in*

- Solid State and Materials Sciences. 2022; 47(2):99-141.
8. Wibowo A, Marsudi MA, Amal MI, Ananda MB, Stephanie R, Ardy H, Diguna LJ. ZnO nanostructured materials for emerging solar cell applications. RSC Advances. 2020;10(70):42838-59.
 9. Cruz DM, Mostafavi E, Vernet-Crua A, Barabadi H, Shah V, Cholula-Díaz JL, Guisbiers G, Webster TJ. Green nanotechnology-based zinc oxide (ZnO) nanomaterials for biomedical applications: A review. Journal of Physics: Materials. 2020;3(3):034005.
 10. Verma R, Pathak S, Srivastava AK, Prawer S, Tomljenovic-Hanic S. ZnO nanomaterials: Green synthesis, toxicity evaluation and new insights in biomedical applications. Journal of Alloys and Compounds. 2021;876:160175.
 11. Le AT, Ahmadipour M, Pung SY. A review on ZnO-based piezoelectric nanogenerators: Synthesis, characterization techniques, performance enhancement and applications. Journal of Alloys and Compounds. 2020;844:156172.
 12. El Golli A, Fendrich M, Bazzanella N, Dridi C, Miotello A, Orlandi M. Wastewater remediation with ZnO photocatalysts: Green synthesis and solar concentration as an economically and environmentally viable route to application. Journal of Environmental Management. 2021;286:112226.
 13. Sharipova A, Slesarenko V, Gutmanas E. Synthesis of metal-metal oxide (Me-MeOm) nanocomposites by partial reduction and cold sintering. Materials Letters. 2020;276:128197.
 14. Panchal P, Paul DR, Sharma A, Choudhary P, Meena P, Nehra SP. Biogenic mediated Ag/ZnO nanocomposites for photocatalytic and antibacterial activities towards disinfection of water. Journal of colloid and interface science. 2020;563:370-80.
 15. Farooq M, Shujah S, Tahir K, Nazir S, Khan AU, Almarhoon ZM, Jevtovic V, Al-Shehri HS, Hussain ST, Ullah A. Ultra efficient 4-Nitrophenol reduction, dye degradation and Cr (VI) adsorption in the presence of phytochemical synthesized Ag/ZnO nanocomposite: A view towards sustainable chemistry. Inorganic Chemistry Communications. 2022;136:109189.
 16. Ramakrishnegowda, Deepu Habbanakuppe, Chandranantha Kampalapura Swamy, BM Anil Kumar, Shobith Rangappa, Kanchugarakoppal S. Rangappa, and Srikantaswamy Shivanna. Ag mediated plasmonic AgO/ZnO composite and its pharmaceutical relevance. Materials Science and Engineering: B. 2023;292:116437.
 17. Sali, Raghavendra K., and Ashok H. Sidarai. Antimicrobial activity and cytotoxic effect of ZnO and Ag-ZnO Nanoparticles Using Capsicum Frutescence Fruits. Bio Nano Science. 2023;13(1):153-166.
 18. Mohamed, Marwa Yousry A., Hela Ferjani, Oluwasayo E. Ogunjinmi, Maroua Jalouli, and Damian C. Onwudiwe. Phyto-mediated synthesis of Ag, ZnO, and Ag/ZnO nanoparticles from leave extract of Solanum macrocarpon: Evaluation of their antioxidant and anticancer activities. Inorganica Chimica Acta. 2024;122086.
 19. Khamidov, Gofur, Ömer Hazman, and Ibrahim Erol. Thermal and biological properties of novel sodium carboxymethylcellulose-PPFMA nanocomposites containing biosynthesized Ag-ZnO hybrid filler. International Journal of Biological Macromolecules 2024; 257:128447.
 20. Shoorgashti, Reyhaneh, Havakhah Shahrzad, Sara Nowroozi, Behnaz Ghadamgahi, Reza Mehrara, and Fatemeh Oroojalian. Evaluation of the antibacterial and cytotoxic activities of Ag/ZnO nanoparticles loaded polycaprolactone/chitosan composites for dental applications. Nanomedicine Journal 2023;10(1).
 21. Slathia S, Gupta T, Chauhan RP. Green synthesis of Ag-ZnO nanocomposite using Azadirachta indica leaf extract exhibiting excellent optical and electrical properties. Physica B: Condensed Matter. 2021; 621:413287.
 22. Karunamoorthy S, Velluchamy M. Design and synthesis of bandgap tailored porous Ag/NiO nanocomposite: an effective visible light active photocatalyst for degradation of organic pollutants. Journal of Materials Science: Materials in Electronics. 2018;23: 20367-82.
 23. Zeng X, Yang Z, Fan M, Cui F, Meng J, Chen H, Chen L. Shape-controlled growth of three-dimensional flower-like ZnO@ Ag composite and its outstanding electrochemical performance for Ni-Zn secondary batteries. Journal of Colloid and Interface Science. 2020;562:518-28.

24. Pandey PK, Chauhan V, Dixit P, Pandey PC. Correlation of enhanced photocurrent with structural and optical properties of Ag–ZnO nanocomposites synthesized by a facile chemical route. *Physica B: Condensed Matter*. 2021;612: 412937.
25. Guo Y, Fu X, Xie Y, Zhu L, Liu R, Liu L. Synthesis of Ag/ZnO nanocomposites with enhanced visible photocatalytic performance. *Optical Materials*. 2022;133: 112980
26. Ezhilarasi AA, Vijaya JJ, Kaviyarasu K, Zhang X, Kennedy LJ. Green synthesis of nickel oxide nanoparticles using *Solanum trilobatum* extract for cytotoxicity, antibacterial and photocatalytic studies. *Surfaces and Interfaces*. 2020;20:100553
27. Chen J, Du D, Yan F, Ju HX, Lian HZ. Electrochemical antitumor drug sensitivity test for leukemia K562 cells at a carbon-nanotube- modified electrode. *Chemistry–A European Journal*. 2005; 11(5):1467-72.

© Copyright (2024): Author(s). The licensee is the journal publisher. This is an Open Access article distributed under the terms of the Creative Commons Attribution License (<http://creativecommons.org/licenses/by/4.0>), which permits unrestricted use, distribution, and reproduction in any medium, provided the original work is properly cited.

Peer-review history:

The peer review history for this paper can be accessed here:

<https://prh.mbimph.com/review-history/3533>